

Published in final edited form as:

Nat Neurosci. 2002 March ; 5(3): 225–233. doi:10.1038/nm808.

## TrkB receptor signaling is required for establishment of GABAergic synapses in the cerebellum

Beatriz Rico, Baoji Xu, and Louis F. Reichardt

Howard Hughes Medical Institute and Department of Physiology, University of California, San Francisco, California 94143, USA

### Abstract

Neurotrophins are essential to the normal development and maintenance of the nervous system. Neurotrophin signaling is mediated by Trk family tyrosine kinases such as TrkA, TrkB and TrkC, as well as by the pan-neurotrophin receptor p75NTR. Here we have deleted the *trkB* gene in cerebellar precursors by Wnt1-driven Cre-mediated recombination to study the function of the TrkB in the cerebellum. Despite the absence of TrkB, the mature cerebellum of mutant mice appears similar to that of wild type, with all types of cell present in normal numbers and positions. Granule and Purkinje cell dendrites appear normal and the former have typical numbers of excitatory synapses. By contrast, inhibitory interneurons are strongly affected: although present in normal numbers, they express reduced amounts of GABAergic markers and develop reduced numbers of GABAergic boutons and synaptic specializations. Thus, TrkB is essential to the development of GABAergic neurons and regulates synapse formation in addition to its role in the development of axon terminals.

---

Four neurotrophins have been identified in mammals: nerve growth factor (NGF), brain-derived neurotrophic factor (BDNF), neurotrophin-3 (NT-3) and neurotrophin-4 (NT-4/5). NGF activates TrkA, BDNF and NT-4/5 activate TrkB, and NT-3 activates TrkC primarily, although it can also activate TrkA and TrkB less efficiently in some cell types (reviewed in ref. <sup>1</sup>).

Analyses of mutant mice show that neurotrophins are important in the survival, differentiation and maintenance of neurons in the PNS, but not in the CNS. Nevertheless, the neurotrophins are attractive candidates for modulating several processes during postnatal development of the CNS, including regulation of dendritic arborization, axonal sprouting and synaptic transmission<sup>2–8</sup>. Despite progress in understanding the functions of neurotrophins in regulating dendritic arborization<sup>6,7</sup>, little is known about their role in synaptogenesis. *In vitro* studies implicate BDNF-mediated activation of TrkB receptors in the development of GABAergic neurons<sup>9–13</sup>. In addition, *in vivo* studies show that overexpression of BDNF accelerates the maturation of cerebellar and cortical inhibitory circuits<sup>14,15</sup>.

The cerebellum is ideal for studies of CNS synaptogenesis. For example, synapses in the granule-cell layer are organized in highly stereotyped structures called glomeruli, which greatly facilitates their analysis at the ultrastructural level. TrkB and BDNF are expressed at high levels in the cerebellum during the postnatal period, including during synaptogenesis<sup>16</sup>. BDNF is expressed in the granule cells and deep cerebellar nuclei<sup>17</sup>, whereas TrkB is expressed at

---

Correspondence should be addressed to L.F.R. (lfr@cgl.ucsf.edu).

#### Competing interests statement

The authors declare that they have no competing financial interests.

Note: See supplementary information on the Nature Neuroscience website ([http://neuroscience.nature.com/web\\_specials](http://neuroscience.nature.com/web_specials)).

different concentrations in Purkinje cells, granule cells, interneurons and glia cells<sup>18,19</sup>. TrkB and its ligands are involved in the development of granule cells<sup>4,20–23</sup>, Purkinje cells<sup>4,23,24</sup> and pontine mossy fibers<sup>25</sup>. The early postnatal mortality of *trkB* and *BDNF* knockout mice prevents studies on the roles of TrkB signaling in cerebellar synaptogenesis, because this process reaches its peak in the second and third postnatal weeks<sup>26</sup>.

To overcome this problem, *trkB* conditional-mutant mice have been generated using the Cre/LoxP recombination system<sup>7,8,27</sup>. Using this system, we have generated mice that lack TrkB expression in the cerebellum by crossing a *trkB* conditional strain<sup>7</sup> with a line of transgenic *Wnt1Cre* mice in which Wnt1 regulatory elements direct the expression of Cre recombinase to the neural crest and primordial midbrain, including the precursors cells of the cerebellum and precerebellar system<sup>28–30</sup>. The *Wnt1Cre/trkB* conditional-mutant mice survive to adulthood with normal numbers of all cerebellar cell types, but have marked deficits in GABAergic enzymes and synapses.

## Results

### Pattern of *Wnt1Cre*-mediated deletion in the cerebellum

The Wnt1 promoter/enhancer is active at embryonic day 8.5 (E8.5) in the region of the neuroepithelium from which all cells in the cerebellum are derived<sup>28</sup>. To determine the pattern of Wnt1-driven Cre-mediated recombination in the cerebellum, we crossed *Wnt1Cre* transgenic mice with mice carrying the Cre reporter *R26R*. In *R26R* mice, expression of  $\beta$ -galactosidase identifies all cells in which Cre-mediated recombination has occurred. Analysis of adult *Wnt1Cre;R26R* mice showed that recombination had occurred in all types of cell in the cerebellum and in most cells in the midbrain, which indicated that progenitor cells committed to these regions expressed the *Wnt1Cre* transgene during development. Some recombination also occurred in other regions of the CNS and PNS (Fig. 1a and b).

We used antibodies against  $\beta$ -galactosidase to examine expression of  $\beta$ -galactosidase in specific cerebellar cell types (Fig. 1c–f). We found that all GABAergic interneurons, Purkinje and granule cells were labeled by  $\beta$ -galactosidase immunostaining (Fig. 1c–f and Supplementary Table 1, available on the supplementary information page of *Nature Neuroscience* online). Although there were examples in which  $\beta$ -galactosidase-containing inclusion bodies were not seen in a confocal section through a cell, inclusions bodies could always be found in other optical sections of that cell.

To confirm that the pattern of recombination found in *Wnt1Cre;R26R* mice was also found in our mutant mice, we examined the expression of  $\beta$ -galactosidase in *Wnt1Cre;fBZ/fBZ* mice carrying two conditional *trkB* alleles. The conditional *fBZ* allele was generated by inserting a loxP-flanked full-length complementary DNA of *trkB*, followed by a *tau-lacZ* cDNA, into the *trkB* locus<sup>8</sup>. Cre-mediated recombination thus eliminated expression of TrkB and activated expression of the *tau-lacZ* reporter under the control of the *trkB* promoter.

Expression of Tau- $\beta$ -galactosidase indicated that Cre-mediated recombination had occurred in the progenitors of several cell types in the adult cerebellum (Fig. 1g–j). As predicted by the above results, recombination occurred in most interneurons in the cerebellum (Fig. 1g and h and Supplementary Table 1). In contrast, none of the antibodies detected immunoreactivity to  $\beta$ -galactosidase in Purkinje and granule-cell bodies, most probably because the Tau- $\beta$ -galactosidase fusion protein is transported into dendrites and axons<sup>31</sup>. The results obtained with *Wnt1Cre;R26R* mice indicated, however, that the *Wnt1Cre* transgenic strain was driving recombination in all cerebellar cell types. Because activity of the Wnt1 promoter precedes the initial appearance of TrkB at postnatal day 7 (P7)<sup>21</sup>, cerebellar neurons almost certainly developed without exposure to signaling mediated by TrkB.

### Loss of TrkB in the cerebellum of *trkB* mutant mice

In agreement with previous studies<sup>18,19</sup>, *in situ* hybridization showed that expression of TrkB varied among different cell types of the cerebellum (Fig. 2a–d). Expression was high in Purkinje cells and Golgi interneurons (Fig. 2a–c), but more moderate in basket and stellate interneurons and in granule cells (Fig. 2c and d).

Because the *Wnt1Cre* transgene was expressed in the progenitors of all cerebellar cell types, we anticipated that *trkB* expression would be lost in *Wnt1Cre;fBZ/fBZ* conditional-mutant mice. *In situ* hybridization showed that there was a complete loss of *trkB* messenger RNA in the cerebellum of adult *Wnt1Cre;fBZ/fBZ* conditional mutants (Fig. 2a–g). An affinity-purified antibody against the extracellular domain of TrkB<sup>32</sup> did not detect TrkB protein in immunoblots of the cerebellum of *Wnt1Cre;fBZ/fBZ* conditional mutants (Fig. 2h). Consistent with previous results<sup>8</sup>, *fBZ/fBZ* mice expressed roughly 25% of the normal amount of full-length TrkB and no truncated isoforms of this protein (Fig. 2h).

### Normal cerebellar architecture without TrkB

To determine the effect of the lack of *trkB* on the cerebellum, we first examined the gross anatomical organization in 2-month-old mutant mice. Analyses of sections stained by Nissl and antibodies specific for glial fibrillary acidic protein (GFAP) indicated that there were no apparent differences in folia development, or in laminar and glial scaffold organization, between wild-type control and conditional-mutant mice (Fig. 3a–h).

Because our study focused on lobule IV (see below), we examined the cross-sectional areas of the molecular and the granule-cell layers in this lobule. Significant reductions in the molecular (24%) and granule cell (16%) layers were observed (Table 1). To determine whether the reductions in cross-sectional areas were caused by reductions in cell number, we quantified the main cell types of the cerebellum. In the granule-cell layer of the conditional mutant, the density of granule cells (the main cell type in this layer) was increased by 12%, whereas the density of Golgi cells was unchanged (Table 1 and Fig. 3f and i). The average diameter of granule cells in mutants was not smaller than in control littermates (Table 1), which suggested that the loss of cross-sectional area was caused by a reduction in the number or size of fibers between these cells. A decrease in fiber number or size would also explain why granule-cell density was increased slightly in mutant animals.

Because the molecular layer contains a very low density of cells, the 24% reduction in its area was almost certainly caused by a loss of dendritic or axonal volume. The cell densities in the molecular layer were similar in all three genotypes (Table 1). We detected no significant changes in the diameter or number of parallel axons profiles (Table 1). A loss of Purkinje cells or reduced volume of Purkinje cell trees might also potentially explain the reduced area of the molecular layer. We observed no significant change in the density of Purkinje cells in *Wnt1Cre;fBZ/fBZ* mutant mice (Table 1 and Fig. 3g and j).

### Granule and Purkinje cell development without TrkB

As in previous studies of *BDNF* and *trkB* mutants<sup>4,22,23</sup>, we observed a modest delay in granule-cell migration in the *trkB* conditional-mutant mice (not shown). Thus, by the end of the third postnatal week, cells had completed migration to the internal granule-cell layer, and both wild-type control and mutant external granule-cell layers appeared identical (not shown). Despite the absence of TrkB, granule-cell development seemed normal. First, the density of granule cells was not reduced in conditional-mutant mice (Table 1). Second, the morphology of granule cells, as observed in Golgi-impregnated sections, appeared normal (Fig. 4a and c). Third, analysis of the ultrastructure of granule cells by electron microscopy indicated that the organization of these cells was normal (Fig. 4b and d). Fourth, the diameters of granule-cell

bodies and the density and diameter of parallel fiber profiles were similar in all three genotypes (Table 1). Last, granule cells seemed to express normal amounts of the  $\alpha 6$  subunit of the GABA<sub>A</sub> receptor (Fig. 4e–h), a molecular marker of maturity and postsynaptic function. Together, these findings suggested that the development of granule cells occurred normally in the absence of TrkB signaling.

Our observations also indicated that the density and distribution of Purkinje cells were normal in adult mutant mice (Fig. 3g and j). In agreement with a previous study of *BDNF* knockout animals<sup>22</sup>, a gross analysis of the Purkinje cell dendritic tree using antibodies specific for calbindin showed that the primary and secondary dendrites were well differentiated (Fig. 4i and j).

### Decreased GAD65 and GAT-1 in *trkB* mutants

Because BDNF mediates the maturation and strength of GABAergic synapses in the cerebellum and visual cortex<sup>14,15</sup>, we extended our analyses to GABAergic cells and fibers. A preliminary analysis of GABAergic innervation in the cerebellum of *trkB* conditional mutants suggested that anterior lobules (such as lobule IV) were more perturbed than posterior lobules (such as lobule VIII), consistent with the suggestion that NT-3 signaling through TrkC may compensate for the lack of TrkB signaling in more posterior lobules<sup>33</sup>. Concentrating on an anterior lobule (lobule IV), we first analyzed the expression of GAD65 (an isoform of the GABA biosynthetic enzyme glutamic acid decarboxylase). GAD65 is localized primarily in presynaptic boutons<sup>34</sup> and the onset of GAD65 expression in the cerebellum seems to follow synaptogenesis<sup>35</sup>.

To rule out the possibility that a phenotype could result from a general delay in the development of the mutant mice, we analyzed the adult cerebellum (P50–P80). Compared with wild-type and *fBZ/fBZ* control littermates, *Wnt1Cre;fBZ/fBZ* conditional-mutant mice showed markedly reduced immunoreactivity to GAD65 in both the granule-cell layer and the molecular layer (Fig. 5a–c, g–i). Because the organization of GAD65-containing boutons in the granule-cell layer made the accurate counting of terminals impractical, we quantified the total labeling found in a defined area (8,600  $\mu\text{m}^2$ ).

Compared with the wild-type control, a marked reduction (~80%) in the area labeled by GAD65 immunostaining was observed in the granule-cell layer of *trkB* conditional mutants (Fig. 6a). For quantitative analyses, the intensities of the immunofluorescent signal for GAD65 were measured and expressed as gray levels. In the granule-cell layer, there was a more than twofold reduction in the number of GAD65-containing particles with high gray levels (>100 units), which suggested that the expression of GAD65 in boutons was also reduced (Fig. 6d). Quantification of this phenotype in the molecular layer, where individual boutons can be identified, showed that, compared with in control mice (wild-type and *fBZ/fBZ*), there was a roughly 75% reduction in the number of GAD65-containing boutons in mutant mice (Fig. 6b). The intensity of GAD65 expression in these boutons was also reduced (Fig. 6e), and the loss of the large-sized boutons (>1.5  $\mu\text{m}$ ) was almost complete (Fig. 6g–i).

To examine whether TrkB function is required only for maintenance and not for initially establishing GABAergic function in the cerebellum, we examined expression of GAD65 at P21—a stage when the process of synaptogenesis in the cerebellum is concluding<sup>26</sup>. At P21, expression of GAD65 was reduced markedly in both the granular and the molecular layer of the mutant cerebellum (not shown).

To confirm a reduction of GABAergic innervation in the mutant cerebellum, we analyzed the expression of the high-affinity plasma membrane GABA transporter GAT-1 in the adult cerebellum<sup>36</sup>. Expression of GAT-1 in the cerebellum is restricted to axon terminals of

GABAergic cells (basket, stellate and Golgi cells), and its onset of expression is simultaneous with the establishment of GABAergic synapses<sup>36</sup>. In agreement with the expression of GAD65, immunoreactivity to GAT-1 was reduced markedly in the molecular and, more prominently, in the granule-cell layer in lobule IV of conditional-mutant mice (Fig. 5d–f and j–l).

Because the inhibitory input from GABAergic interneurons was impaired markedly in the mutant mice, we examined whether GABAergic projections from the cerebellum were also disturbed. We focused our analysis on the fastigial nucleus, which is the main target of the GABAergic axons of Purkinje cells located in anterior lobules of the cerebellum. A roughly 70% reduction in the area of GAD65 immunostaining was found in the fastigial nucleus of *Wnt1Cre;fBZ/fBZ* mice (Figs. 5m–o and 6c). A decrease in the intensity of the remaining GAD65 terminals was also observed in the fastigial nucleus of the mutant mice (Fig. 6f).

### Reductions in symmetric synapses in *trkB* mutants

The reduction of GABAergic markers in cerebella lacking TrkB suggested that TrkB is required for establishing inhibitory neurotransmission. To examine inhibitory synapses more directly, we analyzed the ultrastructure of GABAergic terminals in the granule-cell layer, where the exceptionally regular synaptic organization of the glomerulus made it possible to compare the organization of the inhibitory input in the presence and absence of TrkB (Fig. 7a). The organization of glomeruli seemed to be similar in all three genotypes examined (Fig. 7b–d); however, quantification of inhibitory (symmetric) synapses indicated a roughly 70% decrease in the number of inhibitory synapses per glomerulus in *Wnt1Cre;fBZ/fBZ* mutant mice (Fig. 7e and i). The number of inhibitory synapses per Golgi neuron terminal was also reduced by about 40% in these mice (Fig. 7f–h, j). Notably, the number of inhibitory synapses per terminal was reduced by 20% in *fBZ/fBZ* mice (Fig. 7f, g, j). As compared with wild-type controls, there was no significant difference in the length of symmetric synaptic densities in *fBZ/fBZ* or *Wnt1Cre;fBZ/fBZ* mice (Table 1).

*In vitro* studies have suggested that BDNF may act as a target-derived trophic factor for basilar pontine mossy fibers<sup>25</sup>. Because Cre was also expressed in the pontine nucleus progenitors (Fig. 1a), we investigated whether the density of glomeruli was affected. A significant 27% reduction in glomeruli density was found in *Wnt1Cre;fBZ/fBZ* mutant mice as compared with wild-type control mice (Fig. 7k). We also quantified the number of excitatory (asymmetric) synapses in the remaining glomeruli (mossy fiber–granule cell synapses). No significant differences in the number of excitatory synapses were found between genotypes, which suggested that the mossy fiber–granule cell dendrite synapses were normal (Fig. 7l). Loss of GABAergic inputs and glomeruli might explain the 16% reduction found in the cross-sectional area of the granule-cell layer. Consistent with the anatomical phenotypes, *Wnt1Cre;fBZ/fBZ* mice were ataxic and had severe deficits in motor coordination (Supplementary Fig. 2, available on the supplementary information page of *Nature Neuroscience* online).

### Discussion

We have examined the role of TrkB in development of the cerebellum by using mice that lack TrkB expression in this structure. In contrast to conventional knockout mice, the *Wnt1Cre;fBZ/fBZ* conditional mutants developed into healthy adults. Absence of TrkB did not reduce the survival of any cerebellar cell population but did reduce the volumes of the granule-cell and molecular layers. Notably, there were significant reductions in expression of the GABA biosynthetic enzyme GAD65 and the GABA transporter GAT-1 within the terminals of GABAergic interneurons and Purkinje cells. Interneurons also formed reduced numbers of nerve terminals and, in the granule-cell layer, fewer inhibitory synapses. The decrease in the number of inhibitory synapses was independent of axon terminal development. By contrast,

the number of excitatory synapses formed on these same glomeruli by mossy fiber afferents appeared normal.

### Development of cerebellar morphology

In targeted animals, the absence of TrkB did not significantly alter the overall morphology, layering or foliation of the adult cerebellum. Deficits in the foliation pattern have been observed previously in BDNF mutants at P14 (ref. <sup>4</sup>). It seems possible that this phenotype is not a direct result of the BDNF mutation because postnatal BDNF mutants fail to thrive and are stunted in development owing to poor breathing and cardiac performance<sup>37,38</sup>.

### Development of granule and Purkinje cells

The absence of TrkB did not reduce the number or normal differentiation of granule cells in targeted animals. By contrast, previous studies have suggested that BDNF signaling to TrkB regulates the survival of granule cells at P8 (ref. <sup>4</sup>). It is possible that compensatory mechanisms might result in a normal final density of granule cells in adult animals, despite elevated apoptosis during development. Alternatively, because malnutrition results in a decreased number of cerebellar granule cells<sup>39</sup>, the elevated apoptosis observed in the BDNF mutants may reflect their poor health. Although our results indicate that TrkB signaling is not necessary for granule-cell survival, TrkB signaling may promote survival in the absence of other factors. Five- to sixfold increases in the apoptosis of granule cells are observed at P14 in mice with compound deficiencies in TrkB and TrkC, but not in animals that are deficient in only one receptor<sup>23</sup>.

Although data suggest that BDNF-mediated TrkB signaling has a direct effect on the differentiation of Purkinje cell primary dendrites in conventional mutants at P8 and P12 (refs. <sup>4, 23</sup>), these dendrites appeared normal in adult *Wnt1Cre;fBZ/fBZ* animals. Because normal primary and secondary dendrites are observed in P17 and older BDNF mutants<sup>22</sup>, we think that delays in development might explain the observations in P8–P14 conventional mutants.

In conditionally targeted mice, the molecular layer area was reduced by 24% in lobule IV despite the apparently normal development of granule and Purkinje cells. It is possible that the parallel fibers may have been shorter in the TrkB-deficient cerebellum. Our analysis measured only their density and diameter and not their length. In addition, although the Purkinje cell dendrites appeared normal in our mutant mice, there might have been subtle effects on the higher-order branches of these dendrites that contributed to the reduction.

It has been suggested that basket, stellate and granule cells are essential to the proper formation of Purkinje dendritic arbors and their planar orientations<sup>40,41</sup>. We have shown here that the absence of TrkB has marked effects on Golgi, basket and stellate interneurons. As a result, the inhibitory circuit mediated by these interneurons is almost certainly impaired. Purkinje and granule cell-specific *Cre* lines are needed to examine the potential subtle roles of TrkB on Purkinje dendritic trees or granule-cell axons independently of this circuit.

### Development of inhibitory synapses

The absence of TrkB resulted in significant deficits in the terminals of interneurons that expressed GABA within the cerebellar cortex and in the terminals of Purkinje cells in the deep cerebellar nuclei. Fewer inhibitory terminals were seen and these had lower amounts of GAD65. In addition, fewer inhibitory synapses were formed by these terminals. Consistent with this, treatment with BDNF enhances inhibitory synaptic transmission *in vitro*<sup>9–13</sup>, and overexpression of BDNF accelerates the maturation of GABAergic inputs in both the visual cortex and cerebellum *in vivo*<sup>14,15</sup>. A recent study suggests that TrkB-mediated signaling may promote the formation of excitatory synapses in some brain regions. In this study,

overexpression of BDNF was shown to increase both the complexity of retinal ganglion cell axonal arbors and the number of GFP-synaptobrevin clusters in these arbors in the optic tectum of *Xenopus* tadpoles<sup>42</sup>.

In adult *Wnt1Cre;fBZ/fBZ* mice, the number of terminals and the total area labeled by antibodies specific for GAD65 were reduced markedly in both the molecular and granule-cell layers. In the molecular layer, only 25–30% of the normal number of GABAergic boutons were detected; in the granule-cell layer, there was a fivefold reduction in the area occupied by GABAergic boutons. Analysis by electron microscopy also suggested that there were fewer GABAergic boutons in the granule-cell layer. We measured 70% fewer inhibitory synaptic specializations per glomerulus, but only 40% fewer inhibitory synaptic specializations per GABAergic bouton. This discrepancy suggests that there was a twofold reduction in the number of boutons contacting each glomerulus.

Our findings show that TrkB signaling has a direct role in controlling the number of GABAergic synapses in healthy animals. First, loss of synaptic contacts occurred in the absence of pre- or postsynaptic neuronal loss. Second, not only was the total number of synapses reduced (which could directly reflect a reduction in the number of axonal branches and terminals), but there was also a reduction in the number of synaptic specializations per terminal. This indicates that TrkB may be involved directly in controlling the number of GABAergic synaptic specializations.

*In vitro* studies suggest that TrkB ligands promote survival and neurite outgrowth by cultured basilar pontine nuclei—the main source of cerebellar mossy fibers<sup>25</sup>. Consistent with this, we observed a modest 27% reduction in the density of glomeruli in lobule IV of *trkB* conditional mutants. The remaining mossy fiber boutons looked morphologically normal and had normal numbers of excitatory synapses. The reduction in mossy fiber bouton number was clearly insufficient to explain the fivefold reduction in the area of GABAergic boutons, as well as the four- to fivefold reduction of inhibitory synapses per glomeruli in the granule-cell layer.

In summary, our results show that TrkB signaling *in vivo* is necessary for several aspects of GABAergic neurotransmission in the cerebellum. TrkB seems to be functioning at two different levels: first, in maintaining the synthesis and uptake of GABA; and second, in regulating the number of terminals per axon and the morphological specializations in synaptic contacts. Deficits to these processes caused by a lack of TrkB almost certainly disrupt cerebellar function.

## Methods

### Transgenic mouse strains

Mice lacking TrkB in the cerebellum were produced by breeding mice carrying a *loxP*-flanked *trkB* allele (*fBZ*)<sup>7</sup> with transgenic mice in which *Wnt1* regulatory elements drive *Cre* recombinase expression (*Wnt1Cre*)<sup>28</sup>. In most experiments, *trkB* conditional mutants were compared with *fBZ/fBZ* and wild-type control littermates.

To analyze the distribution of recombination, we generated mice heterozygous for both the *Wnt1Cre* transgene and the *R26R* reporter<sup>43</sup>. Animal procedures were approved by the University of California San Francisco Committee on Animal Research.

### Immunoblot analysis and immunohistochemistry

Protein extracts were prepared from the cerebellum of wild-type, *fBZ/fBZ* and *Wnt1;fBZ/fBZ* mice. We used 10 µg of protein per lane for SDS-PAGE and immunoblots. Antibodies against

the TrkB extracellular domain<sup>32</sup> and against  $\beta$ -tubulin (Sigma, St. Louis, Missouri; 1:400) were used sequentially on the same blot.

For immunohistochemistry, animals were deeply anesthetized and perfused with PBS (pH 7.4), followed by 4% paraformaldehyde in PBS and a series of sucrose-PBS solutions (15–30%). We cut 40- $\mu$ m serial sagittal sections in a sliding microtome. Littermates were processed in parallel in each experimental group ( $n = 3$ ).

For double immunohistochemistry, free-floating sections were preincubated in 5% bovine serum albumen (BSA), 0.3% Triton X-100 diluted in PBS for 1 h at room temperature, and then incubated for 36 h at 4 °C with primary antisera diluted in 1% BSA, 0.3% Triton X-100 in PBS.

Cocktails included monoclonal (Promega, Madison, Wisconsin; 1:1,000) or polyclonal (5 prime–3 prime, Boulder, Colorado; 1:5,000) antibodies against  $\beta$ -galactosidase and one of the following antisera: mouse calbindin-specific antibody (Sigma; 1:1,000), rabbit calbindin-specific antibody (Swant, Bellinzona, Switzerland, 1:1,000), mouse parvalbumin-specific antibody (Sigma; 1:1,000), rabbit parvalbumin-specific antibody (Swant; 1:1,000), rabbit GABA-specific antibody (Sigma; 1:2,000), mouse GFAP-specific antibody (Chemicon, Temecula, California; 1:1,000), mouse phosphorylated neurofilament-specific antibody (NF200, Sigma; 1:2,000), mouse GAD65-specific antibody (Roche, Indianapolis, Indiana; 1:500), rabbit GAT-1-specific antibody (N. Brecha, Univ. California Los Angeles; 1:1,000) and an affinity-purified rabbit antibody against the  $\alpha 6$  subunit GABA<sub>A</sub> receptor (A. Stephenson, University of London; 0.5  $\mu$ g/ml).

Both monoclonal and polyclonal antibodies against  $\beta$ -galactosidase labeled the same cell types. We then rinsed sections and incubated them in the appropriate secondary antibodies: goat antibodies against either mouse or rabbit Alexa 488 and Texas Red (Molecular Probes) diluted in the same solution as the primary antibodies.

### Quantification of fluorescence intensity and cell counts

We examined GAD65-immunoreactive boutons with a Bio-Rad MRC 1000 confocal microscope (100 $\times$ , n.a. 1.30 Plan-Neofluor). The same fields were selected for all genotypes. Two images spaced 1- $\mu$ m apart were used to quantify the fluorescence intensity from each sample ( $n = 3$ ). All images were taken by Kalman averaging (four times) by excitation at 568 nm (laser power 3%, iris 2.4). To obtain binary images, we also used the background threshold of the wild-type sections for the corresponding sections from *fBZ/fBZ* and *Wnt1Cre;fBZ/fBZ* littermates. For particle analysis, the threshold was set at 13 pixels, which was the estimated minimum size of a GAD65 bouton in the *Wnt1Cre;fBZ/fBZ* mutant mice. We measured the fluorescent intensities (gray levels) and the immunolabeled regions in an area of 8,600  $\mu$ m<sup>2</sup>, using NIH Image software as described<sup>44</sup>.

Quantification of the cell counts is described in the Supplementary Methods (available on the supplementary information page of *Nature Neuroscience* online).

### Golgi staining and *in situ* hybridization

We stained brains by the rapid Golgi method<sup>45</sup>. *In situ* hybridization was done with digoxigenin-labeled riboprobes on 100- $\mu$ m sections as described<sup>46</sup>. We used antisense riboprobes to both the extracellular and tyrosine kinase domains of *trkB*. Specificity of the probes was established by using sense probes as controls.

## Electron microscopy

Mice were perfused with 0.9% NaCl, followed by 2.5% glutaraldehyde and 1% paraformaldehyde in 0.1 M sodium cacodylate buffer, pH 7.4, for 20–30 min. The heads were removed and stored overnight at 4 °C, and then each cerebellar lobule was dissected out and postfixed for 1 h in 2% osmium tetroxide, 0.1 M sodium cacodylate, pH 7.4. The lobules were then dehydrated using a series of ethanol dilutions and flat-embedded in an Epon-Araldite mixture. We used semithin sections stained with toluidine blue to identify and trim the medial sagittal plane of lobule IV. Ultrathin sections were cut and stained with uranyl acetate and lead citrate. Quantitative analyses were done blind to genotype. We took 15 electron micrographs from the glomeruli at a final magnification of 35,000× for each genotype in each experiment ( $n = 3$ ). Inhibitory Golgi cell synapses were identified by the criteria given in ref. <sup>47</sup>. The total numbers of symmetric synapses per glomerulus and per Golgi axon varicosity were counted. We measured the diameter of each granule cell in its longest axis (10 cells per genotype per experiment;  $n = 3$ ). We used 10 electron micrographs of the molecular layer at a final magnification of 35,000× for each genotype to analyze parallel fibers in each experiment ( $n = 3$ ). The diameter of the fiber was measured in its longest axis (10 fiber profiles per micrograph). For counting numbers of glomeruli and excitatory synaptic specializations (asymmetric synapses), we used 20 electron micrographs from the granule-cell layer at a final magnification of 7,500× for each genotype in each experiment ( $n = 3$ ).

## Supplementary Material

Refer to Web version on PubMed Central for supplementary material.

## Acknowledgments

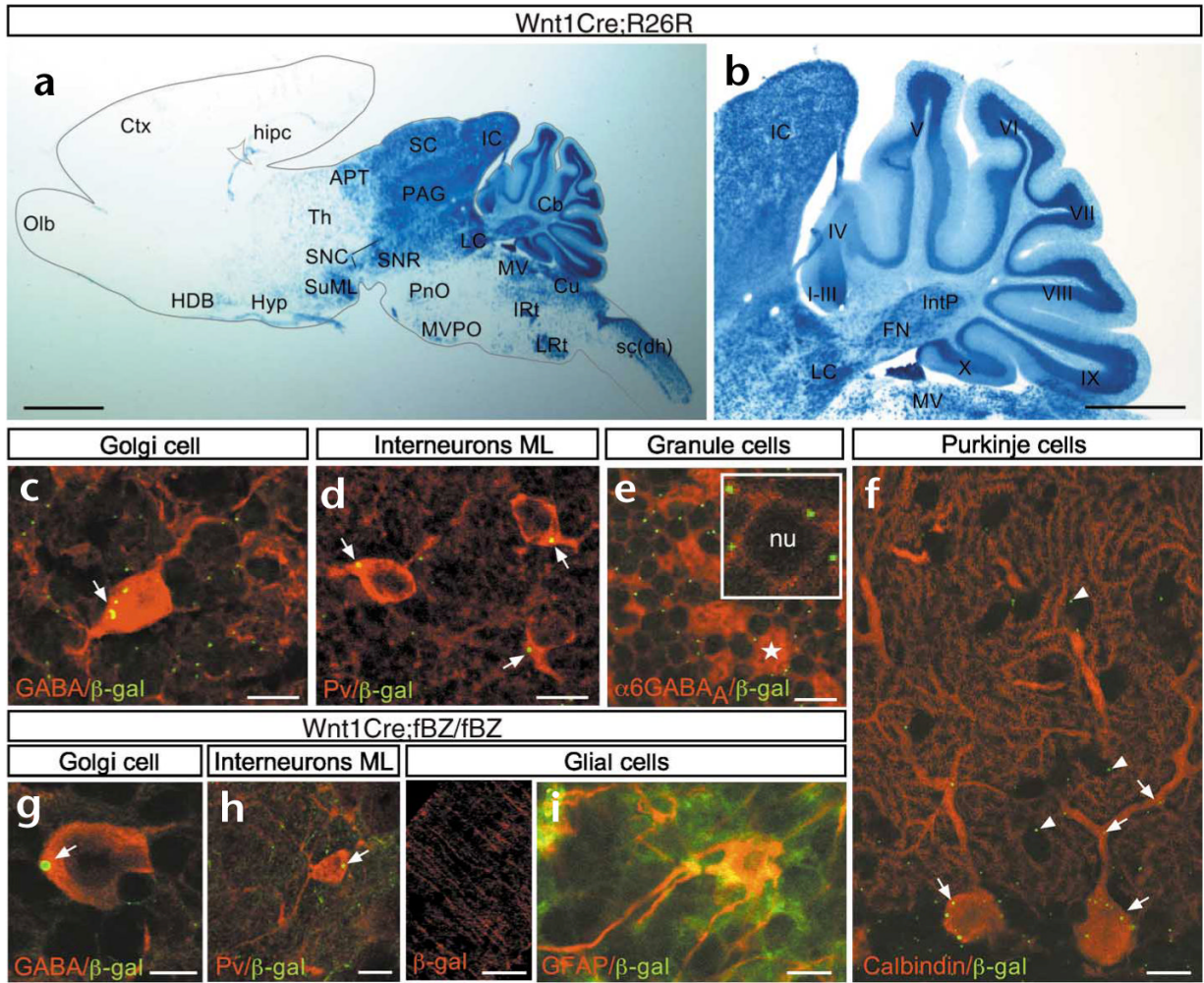
We thank A. P. McMahon and P. Soriano for the Wnt1Cre and R26R transgenic mice; O. Marín, M. Stryker, S. Bamji, L. Elia, T. Elul, U. Fünfschilling and J. Zhu for comments on the manuscript; S. Huling, and I. Hsie for assistance with electron microscopy; N. Brecha for the antibody against GAT-1; and A. Stephenson for the antibody against the  $\alpha 6$  subunit of the GABA<sub>A</sub> receptor. This work was supported by a grant from the USPH and by the HHMI. B.R. was supported by a postdoctoral fellowship from the Ministerio de Educación, Spain. L.F.R. is an Investigator of the HHMI.

## References

- Huang EJ, Reichardt LF. Neurotrophins: roles in neuronal development and function. *Annu Rev Neurosci* 2001;24:677–736. [PubMed: 11520916]
- Lohof AM, Ip NY, Poo MM. Potentiation of developing neuromuscular synapses by the neurotrophins NT-3 and BDNF. *Nature* 1993;363:350–353. [PubMed: 8497318]
- Cohen-Cory S, Fraser SE. Effects of brain-derived neurotrophic factor on optic axon branching and remodelling *in vivo*. *Nature* 1995;378:192–196. [PubMed: 7477323]
- Schwartz PM, Borghesani PR, Levy RL, Pomeroy SL, Segal RA. Abnormal cerebellar development and foliation in BDNF<sup>-/-</sup> mice reveals a role for neurotrophins in CNS patterning. *Neuron* 1997;19:269–281. [PubMed: 9292718]
- Martínez A, et al. TrkB and TrkC signaling are required for maturation and synaptogenesis of hippocampal connections. *J Neurosci* 1998;18:7336–7350. [PubMed: 9736654]
- McAllister AK, Katz LC, Lo DC. Neurotrophins and synaptic plasticity. *Annu Rev Neurosci* 1999;22:295–318. [PubMed: 10202541]
- Xu B, et al. Cortical degeneration in the absence of neurotrophin signaling: dendritic retraction and neuronal loss after removal of the receptor TrkB. *Neuron* 2000;26:233–245. [PubMed: 10798407]
- Xu B, et al. The role of brain-derived neurotrophic factor receptors in the mature hippocampus: modulation of long-term potentiation through a presynaptic mechanism involving TrkB. *J Neurosci* 2000;20:6888–6897. [PubMed: 10995833]
- Mizuno K, Carnahan J, Nawa H. Brain-derived neurotrophic factor promotes differentiation of striatal gabaergic neurons. *Dev Biol* 1994;165:243–256. [PubMed: 8088442]

10. Widmer HR, Hefti F. Stimulation of GABAergic neuron differentiation by NT-4/5 in cultures of rat cerebral cortex. *Dev Brain Res* 1994;80:279–284. [PubMed: 7955354]
11. Vicario-Abejón C, Collín C, McKay RDG, Segal M. Neurotrophins induce formation of functional excitatory and inhibitory synapses between cultured hippocampal neurons. *J Neurosci* 1998;18:7256–7271. [PubMed: 9736647]
12. Seil FJ, Drake-Baumann R. TrkB receptor ligands promote activity-dependent inhibitory synaptogenesis. *J Neurosci* 2000;20:5367–5373. [PubMed: 10884321]
13. Marty S, Wehrle R, Sotelo C. Neuronal activity and brain-derived neurotrophic factor regulate the density of inhibitory synapses in organotypic slice cultures of postnatal hippocampus. *J Neurosci* 2000;20:8087–8095. [PubMed: 11050130]
14. Bao SW, Chen L, Qiao XX, Thompson RF. Transgenic brain-derived neurotrophic factor modulates a developing cerebellar inhibitory synapse. *Learn Memory* 1999;6:276–283.
15. Huang ZJ, et al. BDNF regulates the maturation of inhibition and the critical period of plasticity in mouse visual cortex. *Cell* 1999;98:739–755. [PubMed: 10499792]
16. Lindholm D, Hamner S, Zirrgiebel U. Neurotrophins and cerebellar development. *Persp Dev Neurol* 1997;5:83–94.
17. Rocamora N, Garcialadona FJ, Palacios JM, Mengod G. Differential expression of brain-derived neurotrophic factor, Neurotrophin-3, and low-affinity nerve growth factor receptor during the postnatal development of the rat cerebellar system. *Mol Brain Res* 1993;17:1–8. [PubMed: 8381892]
18. Klein R, et al. Targeted disruption of the TrkB neurotrophin receptor gene results in nervous system lesions and neonatal death. *Cell* 1993;75:113–122. [PubMed: 8402890]
19. Yan Q, et al. Immunocytochemical localization of TrkB in the central nervous system of the adult rat. *J Comp Neurol* 1997;378:135–157. [PubMed: 9120052]
20. Segal RA, Takahashi H, McKay RDG. Changes in neurotrophin responsiveness during the development of cerebellar granule neurons. *Neuron* 1992;9:1041–1052. [PubMed: 1463606]
21. Gao WQ, Zheng JL, Karihaloo M. Neurotrophin-4/5 (NT-4/5) and brain-derived neurotrophic factor (BDNF) act at later stages of cerebellar granule cell differentiation. *J Neurosci* 1995;15:2656–2667. [PubMed: 7722620]
22. Jones KR, Fariñas I, Backus C, Reichardt LF. Targeted disruption of the BDNF gene perturbs brain and sensory neuron development but not motor neuron development. *Cell* 1994;76:989–999. [PubMed: 8137432]
23. Minichiello L, Klein R. TrkB and TrkC neurotrophin receptors cooperate in promoting survival of hippocampal and cerebellar granule neurons. *Genes Dev* 1996;10:2849–2858. [PubMed: 8918886]
24. Shimada A, Mason CA, Morrison ME. TrkB signaling modulates spine density and morphology independent of dendrite structure in cultured neonatal Purkinje cells. *J Neurosci* 1998;18:8559–8570. [PubMed: 9786964]
25. Rabacchi SA, et al. BDNF and NT4/5 promote survival and neurite outgrowth of pontocerebellar mossy fiber neurons. *J Neurobiol* 1999;40:254–269. [PubMed: 10413455]
26. Altman, J.; Bayer, SA. Relation to its Evolution, Structure, and Functions. CRC; Boca Raton, Florida: 1997. *Development of the Cerebellar System*.
27. Minichiello L, et al. Essential role for TrkB receptors in hippocampus-mediated learning. *Neuron* 1999;24:401–414. [PubMed: 10571233]
28. Danielian PS, Muccino D, Rowitch DH, Michael SK, McMahon AP. Modification of gene activity in mouse embryos in utero by a tamoxifen-inducible form of Cre recombinase. *Curr Biol* 1998;8:1323–1326. [PubMed: 9843687]
29. Chai Y, et al. Fate of the mammalian cranial neural crest during tooth and mandibular morphogenesis. *Development* 2000;127:1671–1679. [PubMed: 10725243]
30. Rodriguez CI, Dymecki SM. Origin of the precerebellar system. *Neuron* 2000;27:475–486. [PubMed: 11055431]
31. Callahan CA, Thomas JB. Tau- $\beta$ -galactosidase, an axon-targeted fusion protein. *Proc Natl Acad Sci USA* 1994;91:5972–5976. [PubMed: 8016099]

32. Huang EJ, et al. Expression of Trk receptors in the developing mouse trigeminal ganglion: *in vivo* evidence for NT-3 activation of TrkA and TrkB in addition to TrkC. *Development* 1999;126:2191–2203. [PubMed: 10207144]
33. Tojo H, et al. Neurotrophin-3 is expressed in the posterior lobe of mouse cerebellum, but does not affect the cerebellar development. *Neurosci Lett* 1995;192:169–172. [PubMed: 7566642]
34. Esclapez M, Tillakaratne NJK, Kaufman DL, Tobin AJ, Houser CR. Comparative localization of two forms of glutamic acid decarboxylase and their mRNAs in rat brain supports the concept of functional differences between the forms. *J Neurosci* 1994;14:1834–1855. [PubMed: 8126575]
35. Greif KF, Erlander MG, Tillakaratne NJK, Tobin AJ. Postnatal expression of glutamate decarboxylases in developing rat cerebellum. *Neurochem Res* 1991;16:235–242. [PubMed: 1780026]
36. Morara S, Brecha NC, Marcotti W, Provini L, Rosina A. Neuronal and glial localization of the GABA transporter GAT-1 in the cerebellar cortex. *Neuroreport* 1996;7:2993–2996. [PubMed: 9116226]
37. Balkowiec A, Katz DM. Brain-derived neurotrophic factor is required for normal development of the central respiratory rhythm in mice. *J Physiol (Lond)* 1998;510:527–533. [PubMed: 9706001]
38. Donovan MJ, et al. Brain derived neurotrophic factor is an endothelial cell survival factor required for intramyocardial vessel stabilization. *Development* 2000;127:4531–4540. [PubMed: 11023857]
39. Ito, M. *The Cerebellum and Neural Control*. Raven; New York: 1984.
40. Altman J. Experimental reorganization of the cerebellar cortex. VI Effects of X-irradiation schedules that allow or prevent cell acquisition after basket cells are formed. *J Comp Neurol* 1976;165:49–64. [PubMed: 1244361]
41. Altman J. Experimental reorganization of the cerebellar cortex. VII Effects of late X-irradiation schedules that interfere with cell acquisition after stellate cells are formed. *J Comp Neurol* 1976;165:65–76. [PubMed: 1244362]
42. Alsina B, Vu T, Cohen-Cory S. Visualizing synapse formation in arborizing optic axons *in vivo*: dynamics and modulation by BDNF. *Nat Neurosci* 2001;4:1093–1101. [PubMed: 11593233]
43. Soriano P. Generalized lacZ expression with the ROSA26 Cre reporter strain. *Nat Genet* 1999;21:70–71. [PubMed: 9916792]
44. Fukuda T, Aika Y, Heizmann CW, Kosaka T. GABAergic axon terminals at perisomatic and dendritic inhibitory sites show different immunoreactivities against two GAD isoforms, GAD67 and GAD65, in the mouse hippocampus: a digitized quantitative analysis. *J Comp Neurol* 1998;399:424–426.
45. Valverde F. The rapid Golgi technique for staining CNS neurons. *Light microscopy. Neurosci Protocols* 1993;1:1–9.
46. Nieto MA, Patel K, Wilkinson DG. *In situ* hybridisation analysis of chick embryos in whole mount and in tissue sections. *Methods Cell Biol* 1996;51:219–235. [PubMed: 8722478]
47. Palay, SL.; Chan-Palay, V. *Cerebellar Cortex: Cytology and Organization*. Springer; New York: 1974.

**Fig. 1.**

Wnt1-driven Cre-mediated deletion of the *R26R* and *trkB* alleles, identified by expression of the reporters *lacZ* and *tau-lacZ*, respectively. **(a–f)** *R26R* allele; **(g–j)** *trkB* allele. **(a)** Sagittal view of the brain showing the expression of *lacZ*. **(b)** Higher magnification of **(a)**. For more detailed information about the nuclei in **(a)** and **(b)**, see the expanded version of Fig. 1a and b (Supplementary Fig. 1) on the supplementary information page of *Nature Neuroscience* online. **(c–f)** Single confocal plane images using monoclonal **(c–h)** or polyclonal **(i, j)** antibodies against β-galactosidase and diverse cell-type markers. **(c, g)** Colocalization of β-galactosidase (green puncta) and GABA (red) in Golgi cells. **(d, h)** Colocalization of β-galactosidase (green puncta) and parvalbumin (red) in interneurons of the molecular layer. **(e)** Colocalization of β-galactosidase (green puncta) and the α6 subunit of the GABA<sub>A</sub> receptor (α6GABA<sub>A</sub>; red) in granule cells. Note the amount of α6 GABA<sub>A</sub> receptor in the glomerulus (asterisks), where granule-cell dendrites are located. Receptor expression is also localized in the thin cytoplasm of the granule cell (inset). **(f)** Colocalization of β-galactosidase (green puncta) and calbindin (red) in Purkinje cells. Note the characteristic expression of β-galactosidase in the space occupied by the interneurons (white triangles). **(i, j)** Localization of β-galactosidase in Bergman glia **(i)** and astroglia **(j)**, identified by morphology **(i)** or expression of GFAP **(j)**. Arrows indicate double-labeled neurons or processes. nu, granule-cell nucleus. Scale bars, 1 mm **(a)**, 500 μm **(b)**, 50 μm **(j)**, 15 μm **(c, f)**, 10 μm **(d, e, g–i)**.

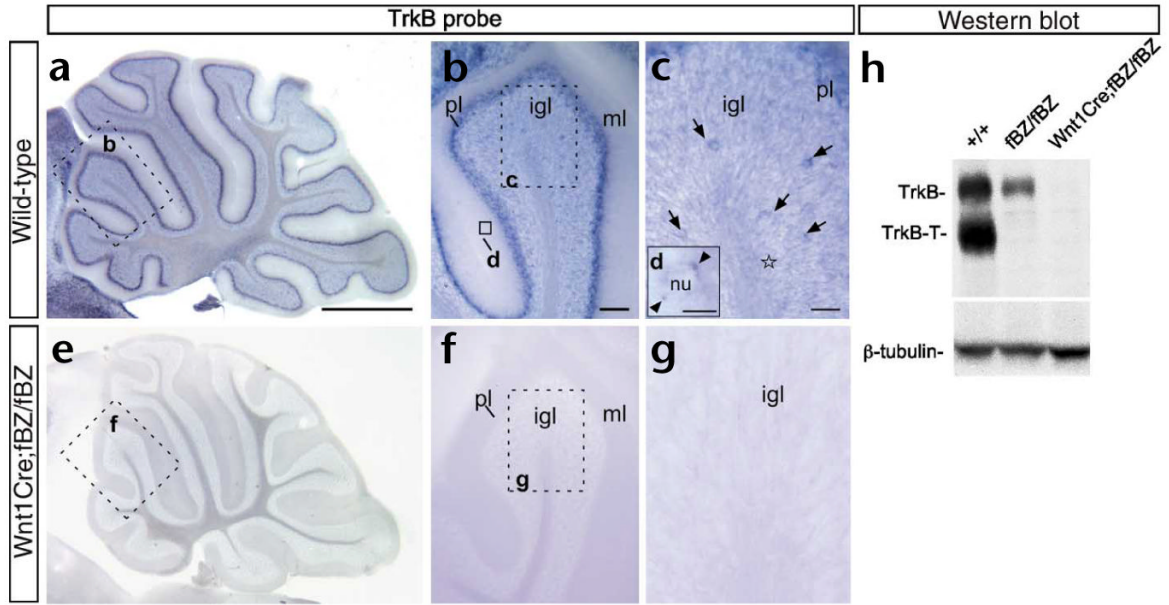


**Fig. 2.**

Loss of TrkB receptor in the cerebellum of *trkB* conditional-mutant mice. (a–g) Sagittal sections showing the expression of TrkB in wild-type (a–d) and *Wnt1;fBZ/fBZ* (e–g) mice at P60. (b, f) Higher-magnification images corresponding to the boxed regions in (a) and (e), respectively. (c, d, g) Higher-magnification images corresponding to the boxed regions in (b) and (f). (b–d) In wild-type controls, expression of TrkB is prominent in Purkinje (pl) and Golgi cells (arrows), but low in granular cells (star) and molecular-layer interneurons (arrowheads). (h) Immunoblot analysis of TrkB receptor protein in the cerebellum of 2-month-old wild-type, *fBZ/fBZ* and *Wnt1;fBZ/fBZ* mice.  $\beta$ -Tubulin protein was used for normalization. igl, internal granule-cell layer; ml, molecular layer; nu, interneuron nucleus; pl, Purkinje cell layer; TrkB, full-length TrkB receptor; TrkB-T, truncated TrkB receptor. Scale bars, 500  $\mu$ m (a, e), 100  $\mu$ m (b, f), 50  $\mu$ m (c, g) and 10  $\mu$ m (d).

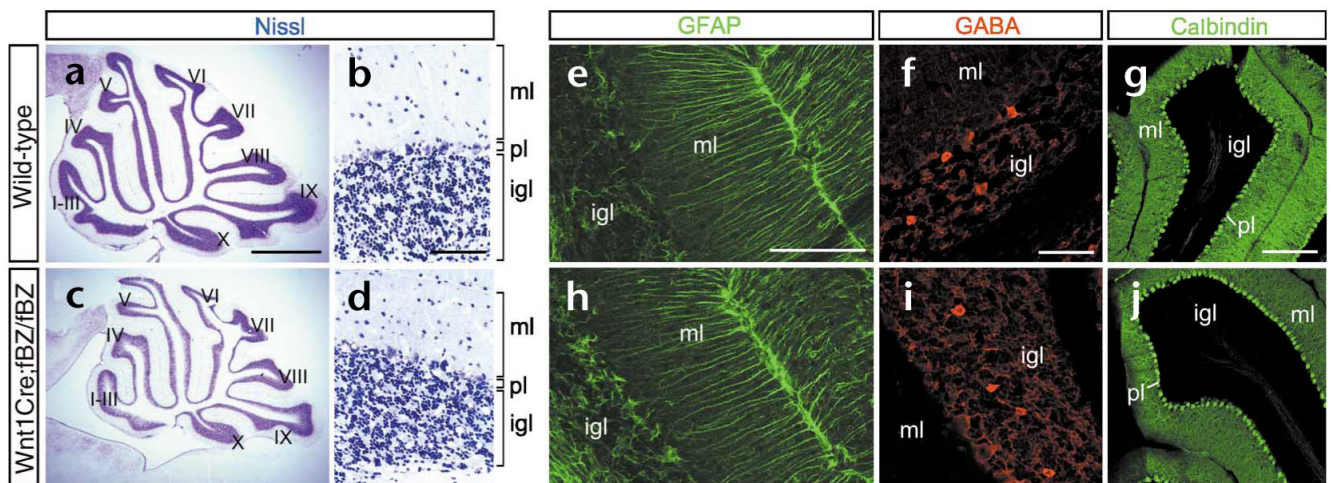


**Fig. 3.** Cerebellar architecture in *trkB* conditional-mutant mice at P50–P80. (a–d) Nissl-stained sagittal sections of wild-type (a, b) and *Wnt1Cre;fBZ/fBZ* (c, d) mice. (b, d) Higher-magnification images from lobule IV. (e–j) Immunohistochemistry of GFAP in wild-type (e) and *Wnt1Cre;fBZ/fBZ* (h) mice, and immunohistochemistry of GABA (f, i) and calbindin (g, j) in wild-type and *Wnt1;fBZ/fBZ* mice. I–X, cerebellar lobules; igl, internal granule-cell layer; ml, molecular layer; pl, Purkinje cell layer. Scale bars, 500  $\mu\text{m}$  (a, c), 100  $\mu\text{m}$  (b, d–f, h, i) and 200  $\mu\text{m}$  (g, j).

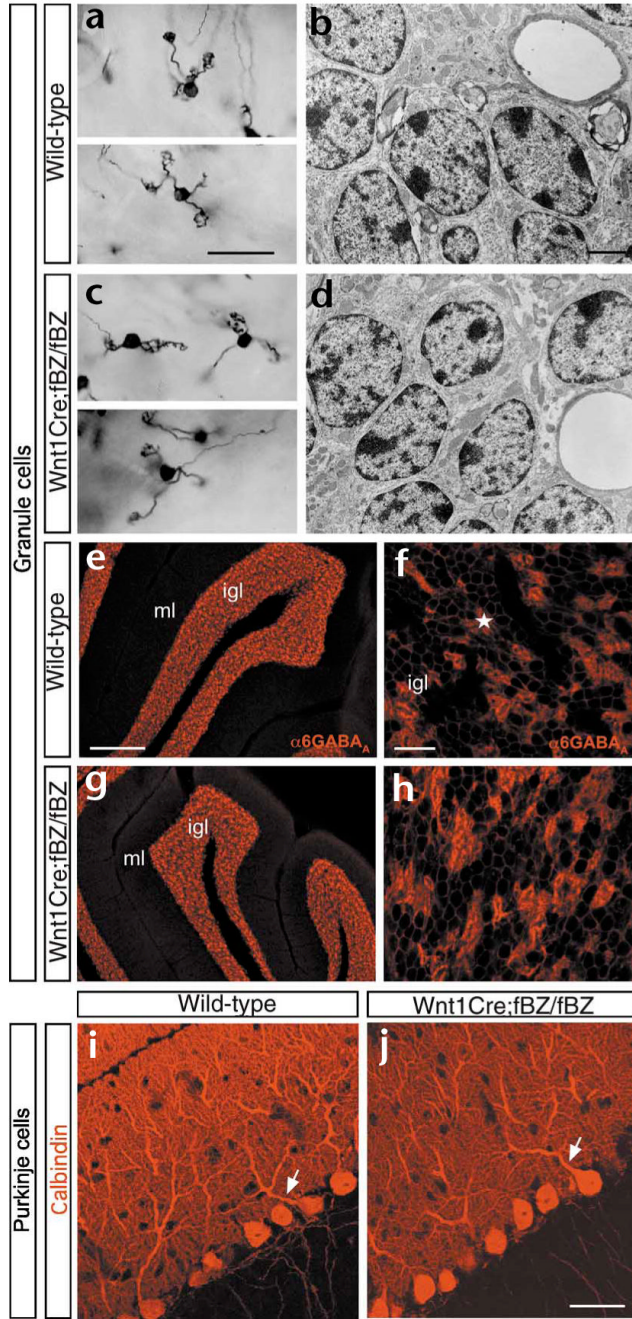


**Fig. 4.** Granular and Purkinje cell morphologies in *trkB* conditional-mutant mice at P50–P80. **(a, c)** Golgi-impregnated sections showing normal body size and typical claw-like telodendria, which are characteristic of differentiated granule cells, in wild-type and *Wnt1Cre;fBZ/fBZ* mice. **(b, d)** Electron microphotographs showing the normal structure in granule cells of wild-type and *Wnt1Cre;fBZ/fBZ* mice. Note that nuclear chromatin is distributed similarly in both genotypes. **(e–h)** Immunohistochemistry of the  $\alpha 6$  subunit of the GABA<sub>A</sub> receptor in lobule IV of wild-type and *Wnt1Cre;fBZ/fBZ* mice. **(f, h)** Higher-magnification images of the internal granule-cell layer shown in **(e)** and **(g)**, respectively. **(i, j)** Purkinje cells at high magnification stained for calbindin. Note the well-differentiated primary dendrites present in both wild-type and

*Wnt1Cre;fBZ/fBZ* mice (arrows). igl, internal granule-cell layer; ml, molecular layer. Scale bars, 20  $\mu\text{m}$  (**a**, **c**, **f**, **h**, **i**, **j**), 2  $\mu\text{m}$  (**b**, **d**) and 200  $\mu\text{m}$  (**e**, **g**).

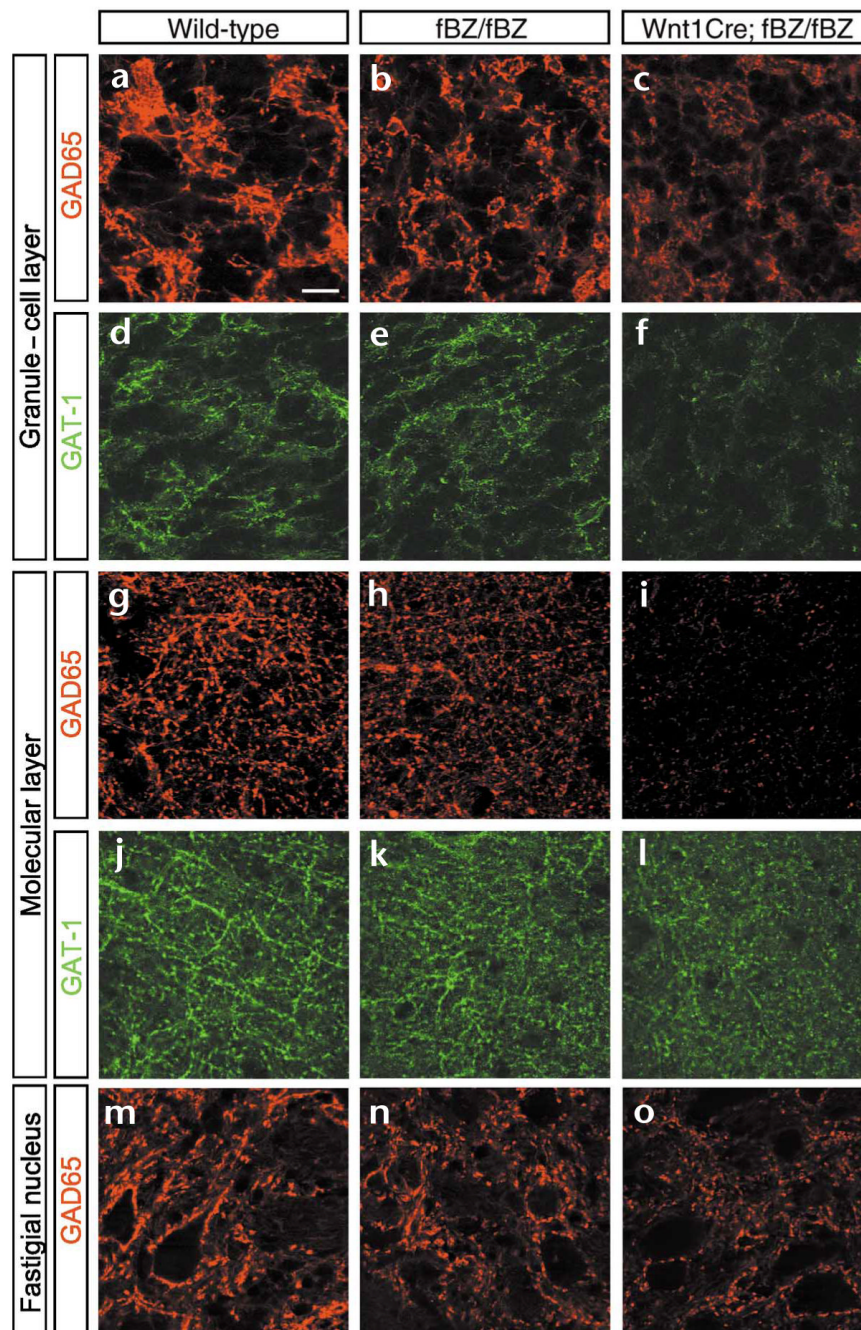


**Fig. 5.** Loss of GABAergic markers in the cerebellum of *trkB* conditional mutant at P50–P80. (**a–f**) Large clusters of GAD65-containing (**a–c**) and GAT-1-containing (**d–f**) boutons derived from Golgi interneurons in the granule-cell layer of lobule IV in wild-type (**a, d**), *fBZ/fBZ* (**b, e**) and *Wnt1;fBZ/fBZ* (**c, f**) mice. (**g–l**) Homogeneous neuropil of individual GAD65-positive (**g–i**) and GAT-1-positive (**j–l**) boutons derived from basket and stellate interneurons in the molecular layer of lobule IV in wild-type (**g, j**), *fBZ/fBZ* (**h, k**) and *Wnt1;fBZ/fBZ* (**i, l**) mice. (**m–o**) Localization of GAD65 in the fastigial nucleus of wild-type (**m**), *fBZ/fBZ* (**n**) and *Wnt1;fBZ/fBZ* (**o**) mice. Scale bar, 25  $\mu$ m (**a–o**).

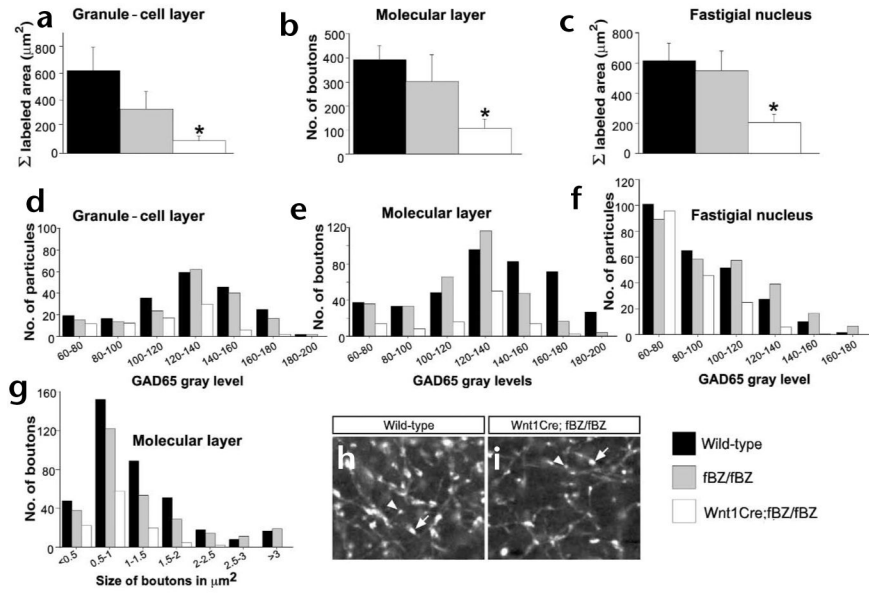


**Fig. 6.** Quantitative analysis of the loss of GABAergic markers in lobule IV and in the fastigial nucleus of *trkB* conditional-mutant mice at P50–P80. **(a)** Quantification of the total area labeled with GAD65-specific antibodies in the granule-cell layers of wild-type, *fBZ/fBZ* and *Wnt1;fBZ/fBZ* mice. **(b)** Quantification of the number of GAD65-labeled boutons in the molecular layer of wild-type, *fBZ/fBZ* and *Wnt1;fBZ/fBZ* mice. **(c)** Quantification of the total area labeled with GAD65-specific antibodies in the fastigial nucleus of wild-type, *fBZ/fBZ* and *Wnt1;fBZ/fBZ* mice. **(d–f)** Histograms comparing the intensities of GAD65 immunostaining (indicated in gray levels) in the granule-cell layer **(d)**, molecular layer **(e)** or fastigial nucleus **(f)** of wild-type, *fBZ/fBZ* and *Wnt1;fBZ/fBZ* mice. **(g)** Quantification of size of GAD65-containing boutons in the molecular layer of wild-type, *fBZ/fBZ* and *Wnt1;fBZ/fBZ* mice. **(h, i)** Sample showing the diverse size of boutons in wild-type **(h)** and *Wnt1;fBZ/fBZ* **(i)** mice. Asterisk denotes a significant difference from the wild-type control ( $n = 3$ ,  $p < 0.03$  **(a)** and  $p < 0.04$  **(c)** by one-way analysis of variance; ANOVA). Data shown are the mean  $\pm$  s.e.m. **(f, g)** Immunohistochemistry of GAD65 in the molecular layer of wild-type **(f)** and *Wnt1;fBZ/fBZ* **(g)** mice. Open triangles indicate small boutons, arrows indicate large boutons. Scale bar, 20  $\mu$ m **(f, g)**.

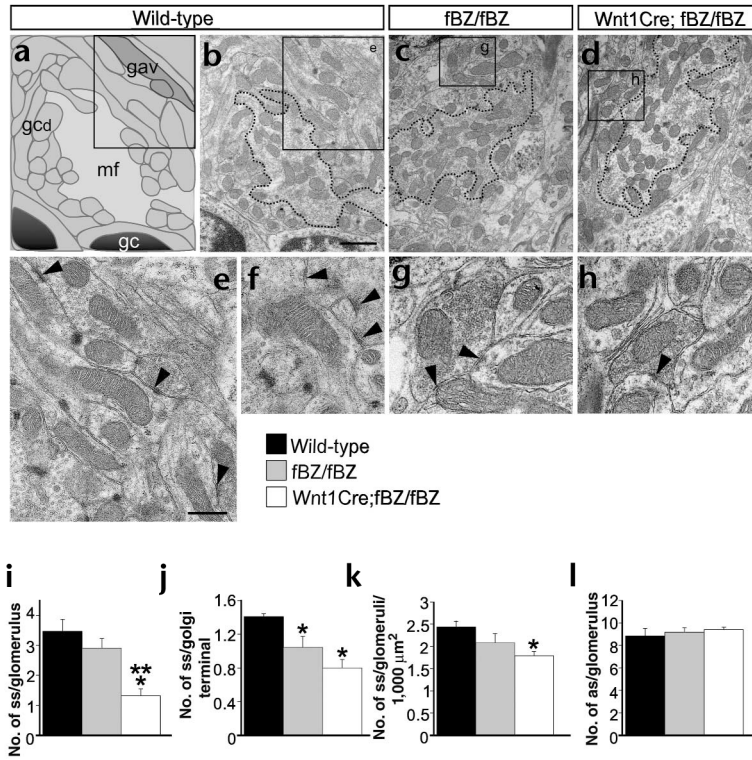


**Fig. 7.** Reduction in the number of symmetric synapses in the granule-cell layer of *trkB* conditional-mutant mice at P50–P80. **(a)** Diagram of the normal organization of the glomerulus. The large mossy fiber (mf) constitutes the center, which is surrounded by dendrites (gcd) of granular cells (gc) and, more externally, by GABAergic Golgi axon varicosities (gav), which synapse onto the granule-cell dendrites. **(b–d)** Fine structure of three representative glomeruli in wild-type, *fBZ/fBZ* and *Wnt1Cre;fBZ/fBZ* mice. Dotted lines indicate the contour of the mossy fiber. **(e, g, h)** Higher-magnification images corresponding to the boxed region in **(b–d)**, respectively, showing symmetric synapses between Golgi axons and granule-cell dendrites (arrowheads). **(f)** Fine structure of a representative glomerulus in wild-type mice, showing that the Golgi axon varicosity forms several synapses in the same terminal. **(i, j)** Quantification of the number of symmetric synapses per glomerulus **(i)** or per Golgi axon varicosity **(j)** in wild-type, *fBZ/fBZ* and *Wnt1Cre;fBZ/fBZ* mice. **(k)** Quantification of the number of glomeruli in 1,000 μm<sup>2</sup>. **(l)** Quantification of the number of asymmetric synapses per glomerulus. Asterisks denote significant differences between the genotype where the asterisk is located and wild-type (\*) or *fBZ/fBZ* (\*\*) mice ( $n = 3$ ,  $p < 0.01$  **(i)** and  $p < 0.05$  **(j)**) by one-way ANOVA. as, asymmetric synapses; ss, symmetric synapses. Data shown are the mean ± s.e.m. Scale bars, 1 μm **(b–d)** and 0.5 μm **(e–h)**.

**Table 1**  
Analysis in the cerebella of *trkB* conditional-mutant mice

Measurement	Genotype	<i>n</i>	(mean ± s.e.m.)	Percentage of wild type
Molecular layer area (IV)	Wild type	3	0.154 ± 0.009 mm <sup>2</sup>	–
	<i>fBZ/fBZ</i>	3	0.161 ± 0.008 mm <sup>2</sup>	–
	<i>Wnt1Cre;fBZ/fBZ</i>	3	0.117 ± 0.004 mm <sup>2</sup> * ** <sup>a</sup>	76* ** <sup>a</sup>
Internal granule-cell layer area (IV)	Wild type	3	0.110 ± 0.005 mm <sup>2</sup>	–
	<i>fBZ/fBZ</i>	3	0.121 ± 0.003 mm <sup>2</sup>	–
	<i>Wnt1Cre;fBZ/fBZ</i>	3	0.092 ± 0.005 mm <sup>2</sup> * ** <sup>a</sup>	84* ** <sup>a</sup>
No. of granule cells per mm <sup>2</sup> (IV)	Wild type	3	1,710.62 ± 41.52	–
	<i>fBZ/fBZ</i>	3	1,711.10 ± 50.71	–
	<i>Wnt1Cre;fBZ/fBZ</i>	3	1,918.04 ± 74.01* ** <sup>b</sup>	112* ** <sup>b</sup>
No. of Golgi cells per mm <sup>2</sup> (IV)	Wild type	3	21.60 ± 3.42	–
	<i>fBZ/fBZ</i>	3	23.27 ± 4.09	–
	<i>Wnt1Cre;fBZ/fBZ</i>	3	27.25 ± 7.57	126
No. of interneurons in molecular layer per mm <sup>2</sup> (IV)	Wild type	3	126.37 ± 4.84	–
	<i>fBZ/fBZ</i>	3	123.55 ± 10.26	–
	<i>Wnt1Cre;fBZ/fBZ</i>	3	122.03 ± 6.64	–
No. of Purkinje cells per mm <sup>2</sup> (IV)	Wild type	3	7.44 ± 0.40	–
	<i>fBZ/fBZ</i>	3	8.44 ± 0.22	–
	<i>Wnt1Cre;fBZ/fBZ</i>	3	7.55 ± 0.48	–
Granule-cell size (diameter, IV, em)	Wild type	3	7.6 ± 0.29 μm	–
	<i>fBZ/fBZ</i>	3	7.4 ± 0.21 μm	–
	<i>Wnt1Cre;fBZ/fBZ</i>	3	7.9 ± 0.18 μm	–
Parallel fiber diameter (IV, em)	Wild type	3	0.223 ± 0.006 μm	–
	<i>fBZ/fBZ</i>	3	0.218 ± 0.007 μm	–
	<i>Wnt1Cre;fBZ/fBZ</i>	3	0.232 ± 0.002 μm	–
No. of parallel fiber profiles per 100 μm <sup>2</sup> (IV, em)	Wild type	3	233.15 ± 30.34	–
	<i>fBZ/fBZ</i>	3	318.30 ± 42.235	–
	<i>Wnt1Cre;fBZ/fBZ</i>	3	287.410 ± 22.474	–
Length of the symmetric synaptic specializations (IV, em)	Wild type	3	0.22 ± 0.012 μm	–
	<i>fBZ/fBZ</i>	3	0.22 ± 0.02 μm	–
	<i>Wnt1Cre;fBZ/fBZ</i>	3	0.20 ± 0.034 μm	–

Asterisks denote significant differences between the genotype and wild-type control (\*) or *fBZ/fBZ* control (\*\*) mice. em, electron microscopy; IV, lobule IV.

<sup>a</sup>One-way ANOVA, *p* < 0.05

<sup>b</sup>One-way ANOVA,  $p < 0.01$ .